IEEE Photonics Journal
An IEEE Photonics Society Publication

Open Access

Widely Tunable Electro-Absorption Modulated V-Cavity Laser

Volume 11, Number 6, December 2019

Sen Zhang
Yimin Xia
Jianjun Meng
Jiasheng Zhao
Jian-Jun He, *Senior Member, IEEE*

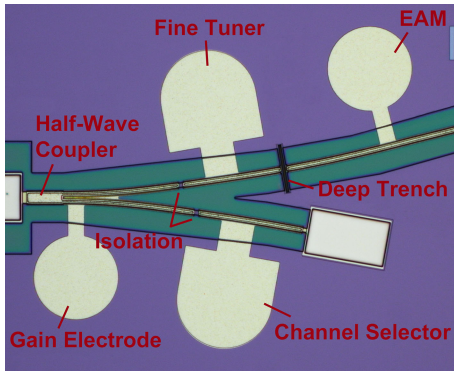

DOI: 10.1109/JPHOT.2019.2950608

Widely Tunable Electro-Absorption Modulated V-Cavity Laser

Sen Zhang,[1] Yimin Xia,[1] Jianjun Meng,[2] Jiasheng Zhao,[2] and Jian-Jun He,[1,2] *Senior Member, IEEE*

[1]State Key Laboratory of Modern Optical Instrumentation, Centre for Integrated Optoelectronics, College of Optical Science and Engineering, Zhejiang University, Hangzhou 310027, China
[2]Lightip Technologies, Company Ltd, Hangzhou 310030, China

DOI:10.1109/JPHOT.2019.2950608

Manuscript received October 19, 2019; accepted October 25, 2019. Date of publication November 4, 2019; date of current version December 16, 2019. This work was supported in part by the National Natural Science Foundation of China under Grant 61535010 and in part by the Strategic Priority Research Program of Chinese Academy of Sciences under Grant XDB24040100. Corresponding author: Jian-Jun He (email: jjhe@zju.edu.cn).

Abstract: We report a widely tunable V-cavity laser monolithically integrated with an electro-absorption modulator (EAM). The device shows a 41-nm wavelength tunability covering 51 channels at 100 GHz spacing on the ITU grid, with a side-mode suppression ratio (SMSR) higher than 47 dB. Error-free transmission over 50 km standard single-mode fiber at 10 Gb/s is demonstrated at all wavelengths over the tuning range. The integrated EAM exhibits a dynamic extinction ratio higher than 12.5 dB. The bit-error-rate measurements show a power penalty less than 3 dB for 50-km transmission. The results demonstrate that this ultra-compact and regrowth-free electro-absorption modulated tunable laser can be a cost-effective transmitter solution for DWDM metropolitan and access networks.

Index Terms: Tunable V-cavity laser, electro-absorption modulated laser, monolithic integration.

1. Introduction

Monolithically integrated widely tunable lasers and electro-absorption modulators (EAM) have been attracting considerable interest as the light sources for long-haul and high-speed fiber-optic communication applications. The EAMs, operating on the basis of the quantum-confined Stark effect (QCSE), have the advantages of compactness, high modulation efficiency and low power consumption. Various monolithic integration schemes have been devised aiming to achieve stable, reliable and efficient electro-absorption modulated lasers (EML), such as butt-joint regrowth (BJR) [1], [2], selective area growth (SAG) [3], dual quantum wells (DQW) [4], offset quantum wells (OQW) [5], asymmetric twin waveguide (ATW) [6], and quantum well intermixing (QWI) [7], [8]. Among these techniques, BJR, SAG and DQW all have a different layer stack for EAM, allowing the quantum wells (QWs) of the laser and modulator to be designed independently for individual optimization. DQW, OQW and QWI only require a single, blanket-type regrowth of the cladding layer. Nevertheless, most of them suffer from sophisticated process control, high fabrication cost and additional coupling loss. To overcome these shortcomings, identical-active-layer (IAL) platform [9]–[11] for InP-based monolithically integrated EMLs has been investigated with benefits of regrowth-free epitaxial process and simple fabrication technology, with the compromise of optical power loss due to the intrinsic absorption in EAMs.

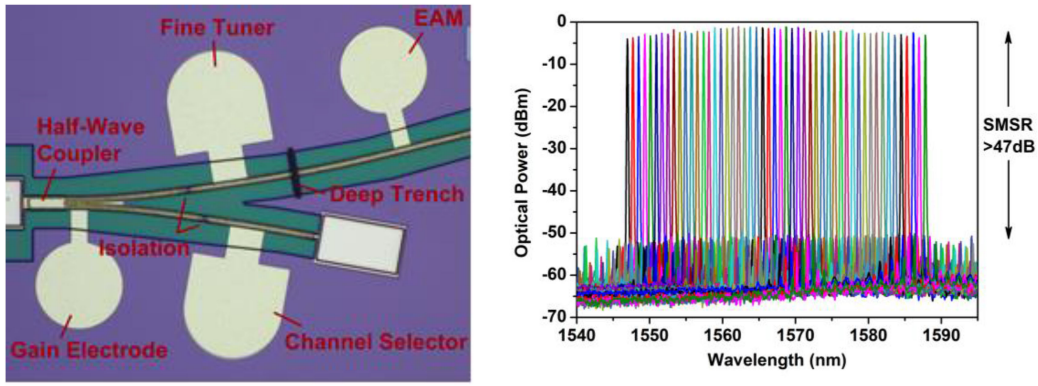

Fig. 1. (a) Top view of the fabricated EMVCL. (b) Superimposed lasing spectra.

Regarding the monolithically integrated widely tunable lasers for full-band tuning in DWDM communication systems, the typical examples reported are primarily based on the structure of sub-wavelength gratings [12], [13] and micro-ring resonators [14]. Grating-assisted tunable lasers require high-resolution lithography and epitaxial regrowth, making it a complex and costly solution difficult to be widely deployed in access and metropolitan networks. Ring-cavity incorporated lasers require strong-confinement ridge etching for InP material because of the obvious waveguide bend, which causes propagation loss for the guided optical modes. Improvements have been made for the device compactness and loss elimination using silicon hybrid integration [15]–[17]. However, such an active-passive heterogeneous integration technology remains immature for high-volume manufacturing, limited by the laser performance and thermal behavior on silicon [17].

Commercially available EMLs are considered as high-cost elements of optical communication systems due to their complex device structures and fabrication processes, even for fixed wavelength DFB based EMLs, not to mention the widely tunable lasers. In order to achieve an ultra-compact and cost-effective device, here we propose a regrowth-free electro-absorption modulated widely tunable V-cavity laser (VCL) for 10-Gb/s DWDM optical links. Thanks to the wide tunability of the grating-free VCL and co-directional gain spectrum shift with temperature, it is shown that the bandgap detuning between the EAM and the laser becomes unnecessary. With a simple fabrication process similar to ordinary Fabry-Perot lasers, the VCL allows a wavelength tuning over a 41-nm range with a side-mode suppression ratio (SMSR) higher than 47 dB. In addition, an error-free transmission up to 50 km at 10 Gb/s is demonstrated.

2. Device Structure and Fabrication

The structure of the electro-absorption modulated V-Cavity Laser (EMVCL) is shown in Fig. 1(a). It comprises a 250 μm long tunable VCL and a 150 μm long EAM connected to the short cavity waveguide of the laser. The footprint of the laser is only about 400 $\times$ 300 μm^2. An identical active layer stack of InGaAlAs-MQW structure is used for both the VCL and EAM sections. The MQW structure consists of five compressively strained 6-nm InGaAlAs QWs sandwiched between 10-nm InGaAlAs barriers. Shallow etched ridge waveguides are used for both the VCL and EAM. Three electrodes are deposited on top of the laser ridge waveguides for current injections. The gain electrode provides optical gain. The channel selector and fine tuner are used for coarse and fine wavelength tuning, respectively, while both partly supplying gain for the two branch cavities [18]. The three electrodes are separated by two isolation gaps. The fabrication process is similar to that of a conventional Fabry-Perot laser, with no epitaxial regrowth or bandgap engineering and no grating. The identical structure for the laser and EAM ensures high coupling efficiency with a maximum mode overlap at the integration interface. A deep trench is introduced for the connection between the laser and the modulator, acting as a partially reflective mirror for the VCL while providing a

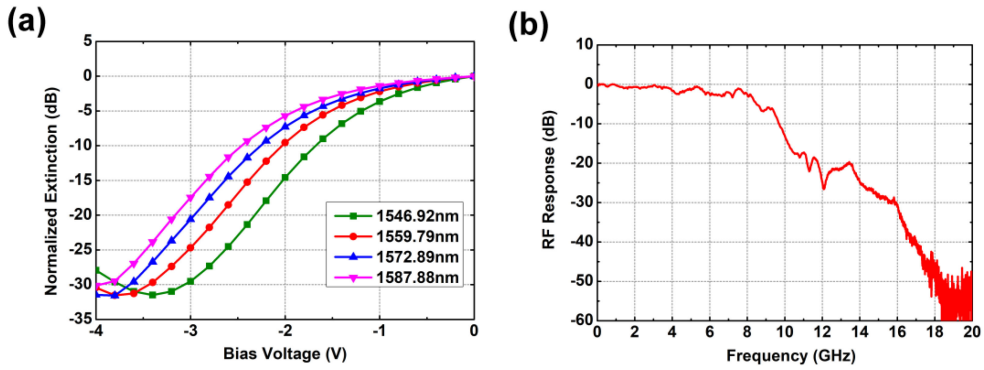

Fig. 2. (a) Static parameters of the integrated EAM. (b) Small signal RF response of the integrated EAM.

good electrical isolation for the EAM. It is designed with an etching depth of 3.5 μm, and a width of 1.9 μm with the optical reflection back into the laser exceeding 50% and the loss lower than 15%. The EAM waveguide inherits the tilt of the laser branch of about 8° to suppress the reflection at the end facet of the chip.

To achieve a high Q factor for the laser resonator, the reflective facets at the back end and the other end of the long cavity are covered with gold, making the reflection strengthened up to nearly 90%. Thus, a better single mode characteristic performance is obtained. The chip is wire-bonded to an aluminum nitride carrier with a parallel 50-Ω impedance-matching termination load.

3. Experimental Results and Discussions

Fig. 1(b) shows the superimposed lasing spectra of 51-channel 100-GHz-spaced wavelengths for the fabricated EMVCL. The channel wavelengths range from 1546.92 nm to 1587.88 nm, matching the ITU-T grids with a coverage of 41 nm. It can cover the entire C or L-Band by blue- or red-shifting the MQW bandgap by about 20 nm, through adjustments of the composition and layer thickness of the quantum wells. The joint electrode for the half-wave coupler of VCL is injected with a CW current of around 50 mA. The other two electrodes on branch waveguides provide currents for channel selection and fine tuning according to the rule of Vernier Effect [19]. Both of them changes from 20 to 80 mA. The TEC controlled temperature varies from 20 to 55 °C while tuning. As demonstrated in [18], at a fixed TEC temperature, a tuning range of $\sim$24 nm can be achieved by varying the current on the channel selector alone. By varying the temperature, the tuning can be extended to over 40 nm. The fiber coupled output power at the on-state with the EAM biased at 0 V ranges from -4 to -1.1 dBm. The laser has a single mode characteristic with the SMSR varying from 47 to 51 dB. The SMSR is about 10 dB higher than previously reported [18], thanks to the higher Q resonators constituted by gold coated reflective facets and the deep trench reflector.

To explore the static modulation characteristics, we measured the extinction ratio as a function of the reverse bias of the EAM with the VCL operating at different wavelengths. Fig. 2(a) shows the static response of the integrated EAM at four different wavelengths. A static extinction ratio larger than 30 dB was obtained due to the existence of an excitonic peak at around -3.5 V bias. This peak shifts to higher reverse bias voltage at longer wavelength, which can be explained by larger wavelength detuning between the modulator bandgap and the operating laser wavelength. For a fixed bias voltage, the static extinction ratio decreases with increasing wavelength due to the increased wavelength detuning between the operating wavelength and the absorption edge. Usually for EAMs integrated with grating based tunable lasers such as a SGDBR laser, there exists a trade-off between the static extinction ratio and the on-state insertion loss due to large wavelength detuning [20]. It may cause significant performance variation at different wavelengths. By contrast,

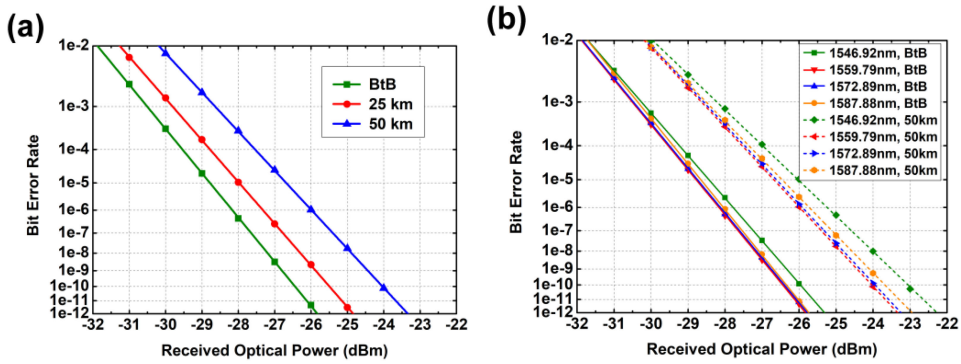

Fig. 3. (a) Bit error rate at the wavelength of 1559.79 nm for different propagation distances. (b) Bit error rate at the four different wavelengths for BtB and 50-km fiber transmission.

the static extinction ratio curve of our device only has small variations with the wavelength. The bias voltage for −15 dB extinction ratio varies from −2 V for 1546.92 nm to −2.8 V for 1587.88 nm. The variation is almost linear with the wavelength and is only about 0.8V for the entire 41 nm wavelength range. This is because the wavelength tuning of the VCL can be extended by the TEC temperature variations [18], which simultaneously tune the absorption edge of the EAM in the same direction as the laser gain spectrum shifts when tuning the wavelength. From the static extinction ratio curves, more than 14 dB extinction ratio can be achieved with a peak-to-peak modulation voltage of 2.0 V by varying the DC bias from −0.9 V for 1546.92 nm to −1.8 V for 1587.88 nm. The insertion loss variation at the on-state varies by less than 3 dB for different wavelengths.

For the dynamic characteristics of the EMVCL, we first measured the small signal response using a Vector Network Analyzer (Anritsu 37369D). As shown in Fig. 2(b), the 3-dB electrical bandwidth of the integrated EAM was measured to be larger than 8 GHz.

For the large signal measurements, the TOSA output was coupled to a single-mode fiber (SMF) without any amplification. A commercial 11.7 GHz high-sensitivity avalanche photodiode (APD) was used for the signal detection. A variable optical attenuator (VOA) was used to control the signal power coupled into the APD. In the eye-diagram and bit-error-rate (BER) measurements, we employed a signal quality analyzer (Model MP1800-A from Anritsu) and a BERT oscilloscope (Model MP2100B from Anritsu). The BERT oscilloscope was used for recording the eye-diagrams. For the transmission measurements over the tuning range, the DC bias point was set each time for optimized eye-diagram and BER. The signal voltage swing was kept constant at 2.0 V for obtaining adequate dynamic extinction ratio at a relatively low-voltage bias point.

Eye-diagrams and BER were measured at different wavelengths within the tuning range with NRZ modulation at a data rate of 10 Gb/s. The generated electrical signal was pseudorandom bit stream (PRBS) with a length of $2^{31}-1$. As shown in Fig. 3(a), BER curves at the wavelength of 1559.79 nm are plotted for back-to-back (BtB), 25-km and 50-km fiber transmission, respectively. For the BtB testing, a received power sensitivity of about −26 dBm was achieved for a BER of 10^{-12}. Error-free propagation was achieved for transmission distance up to 50 km, with the power penalty of 1 dB for 25 km and 2.5 dB for 50 km. Fig. 3(b) displays the superimposed BER curves at the four wavelengths mentioned above for BtB and 50-km fiber transmission, respectively. The BtB received power sensitivity at the BER of 10^{-12} is lower than −25 dBm for all measured wavelengths, and at the same time the power penalty is less than 3 dB after propagating through 50-km SMF. In fact, the modulator has a positive chirp leading to the non-negligible power penalty. However, the penalty with increasing transmission distance is much smaller compared to the case of direct modulation [21], indicating much smaller wavelength chirp. The larger penalty at the shortest wavelength of 1546.92 nm within the whole 41-nm tuning range is mainly due to its lower signal power.

Fig. 4 exhibits the measured eye-diagrams at the four wavelengths for BtB, 25-km and 50-km fiber transmission, respectively. The eye shapes are of little difference for different wavelengths. The

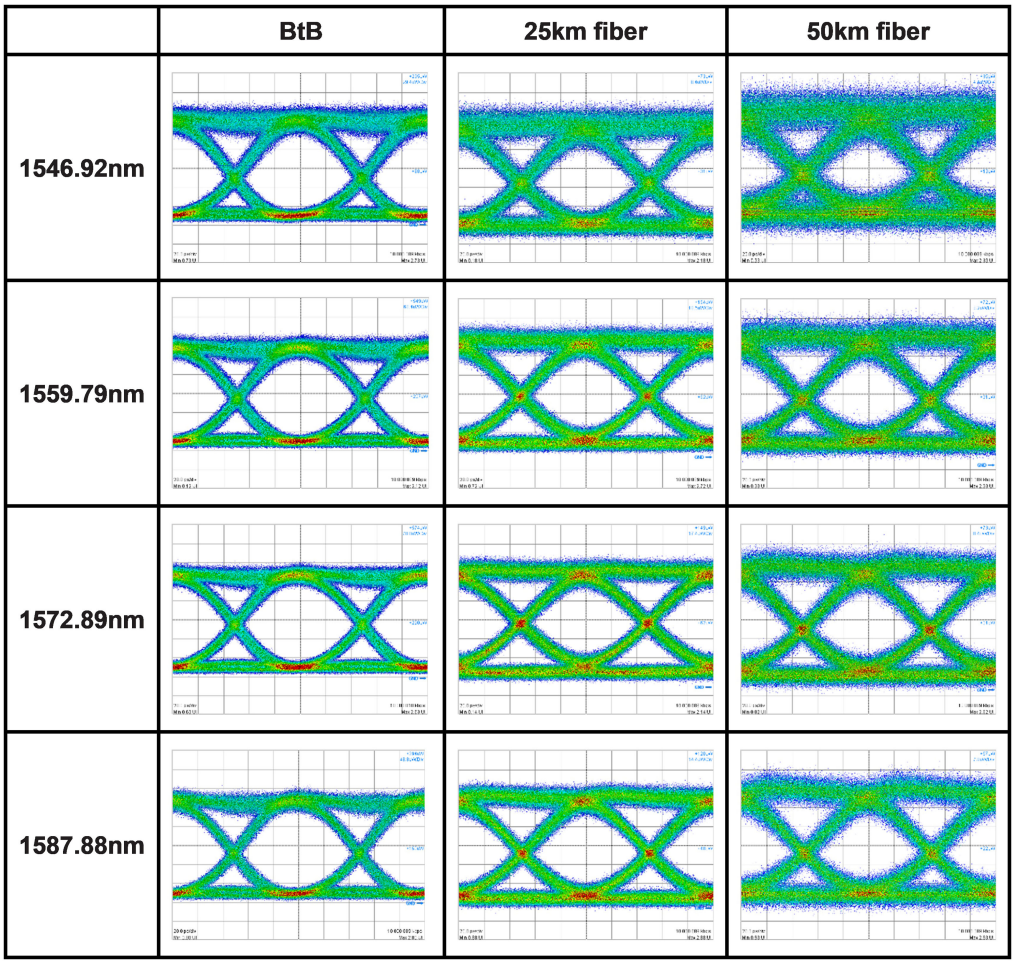

Fig. 4. Eye-diagrams at different wavelengths for various propagation distances.

dynamic extinction ratio is higher than 12.5 dB and the signal to noise ratio is higher than 11.5 dB in back-to-back case. Even after a 50-km fiber transmission the eye remains well open. The noise increases because the received power has decreased. The error-free transmission is possible for longer distances by integrating a power booster amplifier after the EAM.

4. Conclusions

We have demonstrated an InP-based electro-absorption modulated widely tunable V-cavity laser. The monolithic integrated EMVCL does not require any epitaxial regrowth or grating, and its footprint is only 400 $\times$ 300 μm^2. The transmitter shows a wide tuning range of 41 nm, and a SMSR more than 47 dB across the entire range. Without amplification and filtering, the transmission at each available wavelength stays error-floor free up to 50 km at 10-Gb/s NRZ modulation, with the power penalty less than 3 dB. Dynamic extinction ratio of higher than 12.5 dB is achieved. The transmission distance can be further extended by integrating a power booster amplifier. The simple fabrication and high compactness of the EMVCL enable it to be widely deployed in low-cost metro and access DWDM networks.

References

[1] W. Kobayashi *et al.*, "Design and fabrication of 10-/40-Gb/s, uncooled electroabsorption modulator integrated DFB laser with butt-joint structure," *J. Lightw. Technol.*, vol. 28, no. 1, pp. 164–171, Jan. 2010.

[2] F. Soares *et al.*, "High-performance InP PIC technology development based on a generic photonic integration foundry," in *Proc. Opt. Fiber Commun. Conf.*, San Diego, CA, USA, Mar. 2018, Paper M3F.3.

[3] L. Han *et al.*, "Electroabsorption-modulated widely tunable DBR laser transmitter for WDM-PONs," *Opt. Exp.*, vol. 22, no. 24, pp. 30368–30376, Dec. 2014.

[4] A. Tauke-Pedretti, M. N. Sysak, J. S. Barton, J. W. Raring, L. Johansson, and L. A. Coldren, "40-Gb/s series-push-pull Mach-Zehnder transmitter on a dual-quantum-well integration platform," *IEEE Photon. Technol. Lett.*, vol. 18, no. 18, pp. 1922–1924, Sep. 2006.

[5] M. L. Masanovic *et al.*, "Widely tunable monolithically integrated all-optical wavelength converters in InP," *J. Lightw. Technol.*, vol. 23, no. 3, pp. 1350–1362, Mar. 2005.

[6] V. M. Menon, F. Xia, and S. Forrest, "Photonic integration using asymmetric twin-waveguide (ATG) technology: Parts I & II," *IEEE J. Sel. Topics Quantum Electron.*, vol. 11, no. 1, pp. 17–42, Jan./Feb. 2005.

[7] E. J. Skogen *et al.*, "Monolithically integrated active components: A quantum-well intermixing approach," *IEEE J. Sel. Topics Quantum Electron.*, vol. 11, no. 2, pp. 343–355, Mar./Apr. 2005.

[8] H. Zhao *et al.*, "High-power indium phosphide photonic integrated circuits," *IEEE J. Sel. Topics Quantum Electron.*, vol. 25, no. 6, Nov./Dec. 2019, Art no. 4500410.

[9] A. Ramdane, F. Devaux, N. Souli, D. Delprat, and A. Ougazzaden, "Monolithic integration of multiple-quantum-well lasers and modulators for high-speed transmission," *IEEE J. Sel. Topics Quantum Electron.*, vol. 2, no. 2, pp. 326–335, Jun. 1996.

[10] L. Hou, M. Tan, M. Haji, I. Eddie, and J. H. Marsh, "EML based on side-wall grating and identical epitaxial layer scheme," *IEEE Photon. Technol. Lett.*, vol. 25, no. 12, pp. 1169–1172, Jun. 2013.

[11] M. Theurer, G. Przyrembel, A. Sigmund, W. D. Molzow, U. Troppenz, and M. Möhrle, "56 Gb/s L-band InGaAlAs ridge waveguide electroabsorption modulated laser with integrated SOA," *Physica Status Solidi A*, vol. 213, no. 4, pp. 970–974, Apr. 2016.

[12] Y. A. Akulova *et al.*, "Widely tunable electroabsorption-modulated sampled-grating DBR laser transmitter," *IEEE J. Sel. Topics Quantum Electron.*, vol. 8, no. 6, pp. 1349–1357, Nov./Dec. 2002.

[13] A. J. Ward *et al.*, "Widely tunable DS-DBR laser with monolithically integrated SOA: Design and performance," *IEEE J. Sel. Topics Quantum Electron.*, vol. 11, no. 1, pp. 149–156, Jan./Feb. 2005.

[14] S. Matsuo and T. Segawa, "Microring-resonator-based widely tunable lasers," *IEEE J. Sel. Topics Quantum Electron.*, vol. 15, no. 3, pp. 545–554, May./Jun. 2009.

[15] J. C. Hulme, J. K. Doylend, and J. E. Bowers, "Widely tunable Vernier ring laser on hybrid silicon," *Opt. Exp.*, vol. 21, no. 17, pp. 19718–19722, Aug. 2013.

[16] N. Kobayashi *et al.*, "Silicon photonic hybrid ring-filter external cavity wavelength tunable lasers," *J. Lightw. Technol.*, vol. 33, no. 6, pp. 1241–1246, Mar. 2015.

[17] G. Duan *et al.*, "Hybrid III–V on silicon lasers for photonic integrated circuits on silicon," *IEEE J. Sel. Topics Quantum Electron.*, vol. 20, no. 4, pp. 158–170, Jul./Aug. 2014.

[18] S. Zhang, J. Meng, S. Guo, L. Wang, and J.-J. He, "Simple and compact V-cavity semiconductor laser with 50×100 GHz wavelength tuning," *Opt. Exp.*, vol. 21, no. 11, pp. 13564–13571, Jun. 2013.

[19] J. Jin, L. Wang, T. Yu, Y. Wang, and J.-J. He, "Widely wavelength switchable V-coupled-cavity semiconductor laser with $\sim$40 dB side-mode suppression ratio," *Opt. Lett.*, vol. 36, no. 21, pp. 4230–4232, Nov. 2011.

[20] M. Trajkovic, F. Blache, H. Debregeas, K. A. Williams, and X. J. M. Leijtens, "Increasing the speed of an InP-based integration platform by introducing high speed electroabsorption modulators," *IEEE J. Sel. Topics Quantum Electron.*, vol. 25, no. 5, Sep./Oct. 2019, Art no. 3400208.

[21] J. Meng *et al.*, "Full C-band tunable V-cavity-laser based TOSA and SFP transceiver modules," *IEEE Photon. Technol. Lett.*, vol. 29, no. 12, pp. 1035–1038, June. 2017.